

Triangular flow in event-by-event ideal hydrodynamics in Au+Au collisions at $\sqrt{s_{NN}} = 200A$ GeV

Hannah Petersen, Guang-You Qin, Steffen A. Bass, and Berndt Müller
Department of Physics, Duke University, Durham, North Carolina 27708-0305, United States

The first calculation of triangular flow v_3 in Au+Au collisions at $\sqrt{s_{NN}} = 200A$ GeV from an event-by-event (3+1)-d transport+hydrodynamics hybrid approach is presented. As a response to the initial triangularity ϵ_3 of the collision zone, v_3 is computed in a similar way to the standard event-plane analysis for elliptic flow v_2 . It is found that the triangular flow exhibits weak centrality dependence and is roughly equal to elliptic flow in most central collisions. We also explore the transverse momentum and rapidity dependence of v_2 and v_3 for charged particles as well as identified particles. We conclude that an event-by-event treatment of the ideal hydrodynamic evolution starting with realistic initial conditions generates the main features expected for triangular flow.

PACS numbers: 25.75.-q, 24.10.Lx, 24.10.Nz

Collective behaviour of particles emitted from relativistic heavy ion collisions, such as elliptic flow, is one of the earliest predicted observables that indicates fluid-like behaviour of the created hot and dense nuclear matter [1–4]. The pressure gradients need to be large enough to translate an early stage coordinate space asymmetry to a final state momentum space anisotropy. Therefore, the high values of the second coefficient of the Fourier expansion of the azimuthal distribution of the particles, v_2 , that have been reported by the experiments at the Relativistic Heavy Ion Collider (RHIC) [5–8] have led to the conclusion that the quark gluon plasma is a nearly perfect liquid [9, 10].

The collective flow observables manifest themselves in multi-particle-correlations as well. For example, the so called cumulant method has been very successful in quantifying the harmonic coefficients of the azimuthal particle distributions [11]. Recently $\Delta\eta$ - $\Delta\phi$ correlations have been explored in a new manner by extracting a triangular flow signal from the data that is responsible for most of the structures that were previously attributed to other mechanisms [12, 13]. Features like long-range rapidity correlations on the near- and away-side accompanied by a conical structure on the away-side have been often referred to in the context of jet-medium interaction. The preliminary PHOBOS data show a long range correlation in rapidity which would be supported by an initial state generated from a flux tube picture like in NEXsphereIO [14, 15]. In this model one is also able to observe the features like the ridge and the "cone" in the two-particle correlations.

The triangular flow, v_3 , is the third coefficient of the Fourier expansion of the azimuthal distribution of the final particles in momentum space with respect to the corresponding event plane angle Ψ_3 that is defined below. This angle fluctuates randomly event by event in contrast to the well-known event plane angle Ψ_2 used for the elliptic flow analysis, which is strongly correlated to the reaction plane. The triangular flow is assumed to be the response to a triangular shape of the initial state, described by a nonzero triangularity, ϵ_3 , that arises from

the fluctuations of the initial collisions.

In contrast to the extensively studied observables like directed flow (v_1), elliptic flow (v_2) and the fourth harmonic (v_4), the triangular flow (v_3) is not correlated to the reaction plane that is defined by the beam axis and the impact parameter axis of the collision. The initial state fluctuations in the transverse plane are random with respect to the reaction plane. In a standard hydrodynamic calculation with smooth initial conditions only the even coefficients of the Fourier expansion are non-zero at midrapidity. The odd coefficients vanish by symmetry in collisions of identical nuclei which is the reason why they have not been studied so far.

In this paper the latest version of the Ultra-relativistic Quantum Molecular Dynamics (UrQMD) [16, 17] together with ideal relativistic fluid dynamics is used to explore this new observable [32]. The full event-by-event setup of this hybrid approach allows to extract a v_3 component from the final particle distributions. The method is very similar to the standard elliptic flow event plane measurement and will be outlined below. Predictions for the impact parameter dependence and the transverse momentum dependence of identified particles are made.

Let us now review the main ingredients of the hybrid approach [18, 19] that are relevant for the development of triangular flow. The initial binary nucleon-nucleon collisions are modeled in UrQMD following the Lund model of nucleon-nucleon reactions [20] involving color flux tubes excitation and fragmentation processes that provide long range rapidity correlations and fluctuations in the energy deposition in the transverse plane. For Au+Au collisions at the highest RHIC energies the starting time for the hydrodynamic evolution has been chosen to be $t_{\text{start}} = 0.5$ fm in order to fit the final pion multiplicity at midrapidity. Only the matter around midrapidity ($|y| < 2$) is considered to be locally thermalized and takes part in the ideal hydrodynamic evolution. The more dilute spectator/corona regions are treated in the hadronic cascade approach throughout the reaction. To map the point particles from the UrQMD initial state to energy, momentum and net baryon density distributions each particle is

represented by a three-dimensional Gaussian distribution [21].

The ideal hydrodynamic evolution [22, 23] for the hot and dense stage of the collision translates the initial fluctuations in the transverse energy density to momentum space distributions. A hadron gas equation of state [24] has been used because we are aiming here only at qualitative statements and not at quantitative comparisons. This equation of state (EoS) has been extensively tested and gives reasonable results for multiplicities and particle spectra. Furthermore, given the same average speed of sound during the evolution, flow observables are not sensitive to the details of the EoS [25, 26].

The transition from the hydrodynamic evolution to the transport approach when the matter is diluted in the late stage is treated as a gradual transition on an approximated constant proper time hyper-surface (see [25, 27] for details). The final rescatterings and resonance decays are taken into account in the hadronic cascade.

The above event-by-event setup includes all the main ingredients that are supposed to be necessary for the build up of triangular flow. Since the complete final state particle distributions are calculated, an analysis similar to those applied by experimentalists is used.

The definition of the participant eccentricity can be generalized to the triangularity defined as

$$\epsilon_n = \frac{\sqrt{\langle r^n \cos(n\phi) \rangle^2 + \langle r^n \sin(n\phi) \rangle^2}}{\langle r^n \rangle} \quad (1)$$

where in contrast to [12] the factor in front of $\cos(3\phi)$ is taken to be r^3 since this is the more consistent way to do the Fourier expansion of the distribution function. (r, ϕ) in this case are polar coordinates corresponding to the transverse plane in coordinate space. We have calculated the triangularity of the UrQMD initial state for all the particles that are newly produced or have undergone at least one interaction and with a rapidity between $-2 < y < 2$ at the starting time of the hydrodynamic evolution ($t_{\text{start}} = 0.5$ fm). The centrality dependence and the values of the eccentricity as well as the triangularity are comparable to those obtained by a Glauber Monte Carlo approach [13] (see Fig. 4).

The particle distribution in coordinate space is then transferred to the final state particle distribution in momentum space by the pressure gradients during the hydrodynamic evolution. Experiments are only able to measure the momenta of the particles but not the coordinates, therefore, one has to find a way to generalize the elliptic flow analysis to triangular flow analysis in a consistent way. We propose here to use the standard event plane method [28] and define an event plane for triangular flow in the following way

$$\Psi_n = \frac{1}{n} \arctan \frac{\langle p_T \sin(n\phi_p) \rangle}{\langle p_T \cos(n\phi_p) \rangle}, \quad (2)$$

where (p_T, ϕ_p) are polar coordinates in momentum space.

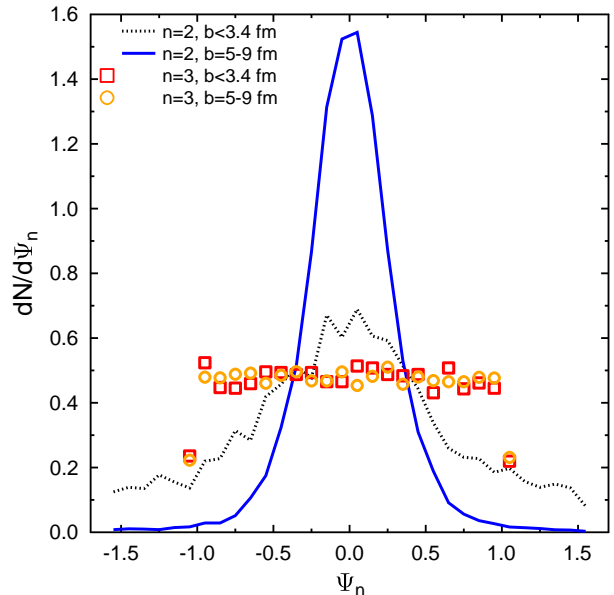


FIG. 1: (Color online) Distribution of event-plane angles Ψ_2 (dotted and full line) and Ψ_3 (open squares and circles) with respect to the reaction plane in central ($b < 3.4$ fm) and mid-central ($b = 5 - 9$ fm) Au+Au collisions at $\sqrt{s_{\text{NN}}} = 200$ A GeV.

As all the details of the final particles are known in our calculation, the resolution of the event plane angle can be improved by taking into account all the particles (also neutral particles) in a certain kinematic range ($|\eta| < 2$) to determine the event plane. The resolution is calculated by comparing two sub events and turns out to be around 0.8 radians for the triangular flow plane angle and 0.7 to 0.95 for the v_2 event plane angle depending on the centrality. This corresponds to an uncertainty in the angle of approximately 12 degrees in mid-central collisions.

The distributions of the resulting event plane angles Ψ_2 and Ψ_3 with respect to the known reaction plane (positive x-direction defines $\Psi = 0$) are shown in Fig. 1. As expected the elliptic flow event plane is Gaussian distributed and therefore correlated to the reaction plane, especially in less central events. The triangular flow plane shows a flat distribution between -60 and $+60$ degrees since the fluctuations that lead to a v_3 component are random with respect to the reaction plane. These internally consistent results increase our confidence in the analysis method proposed here.

To explore the correlation between the initial spatial event plane and the corresponding final event plane we define an initial event plane angle Φ_n in analogy to Eq. (2):

$$\Phi_n = \frac{1}{n} \arctan \frac{\langle r^n \sin(n\phi) \rangle}{\langle r^n \cos(n\phi) \rangle}. \quad (3)$$

For elliptic flow this angle is the one that defines the so called participant plane. With the used conventions Φ_n is defined in the region between $-\pi/n$ and $+\pi/n$. For convenience, we introduce a shifted angle $\Phi'_n = \Phi_n + \pi/n \pmod{2\pi/n}$, defined in the domain $-\pi/n < \Phi'_n < +\pi/n$.

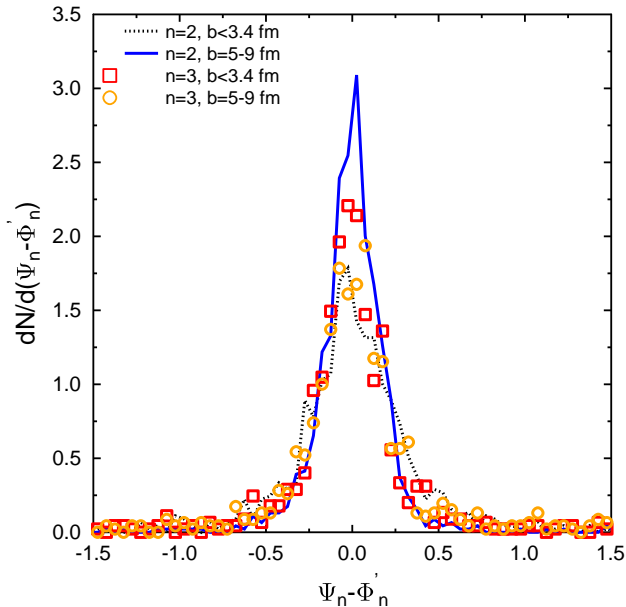


FIG. 2: (Color online) Correlation of the final event plane angles Ψ_2 (dotted and full line) and Ψ_3 (open squares and circles) with the corresponding initial event plane angles Φ'_2 and Φ'_3 in central ($b < 3.4$ fm) and mid-central ($b = 5 - 9$ fm) Au+Au collisions at $\sqrt{s_{NN}} = 200$ A GeV.

The correlation between the final (Ψ_n) and initial (Φ'_n) event planes for two different centrality classes is shown in Fig. 2. There is a strong correlation in all four cases which has a similar shape. For elliptic flow there is a stronger contribution from the collision geometry that results in a centrality dependence of the correlation ($\Psi_2 - \Phi'_2$) [29]. In more central collisions most of the elliptic flow comes from fluctuations while in more peripheral events the almond-shape geometry of the collision zone has a major effect on v_2 which leads to an even stronger correlation of the two angles. For the triangular flow the distribution is very similar for central and mid-central events since it is only caused by fluctuations in both cases. This analysis has been carried out on an event by event basis and confirms that the final triangular flow is related to the initial triangularity.

Further evidence for a strong correlation between initial state geometry and the final state momentum anisotropies is found by looking at the flow coefficients as a function of the corresponding ϵ_n . The flow coefficients are calculated by using the following formula

$$v_n = \langle \cos(n(\phi_p - \Psi_n)) \rangle \quad (4)$$

where it is important to note that the particle that is correlated to the event plane is removed from the event plane determination to eliminate auto-correlations. The final results for v_n are obtained by dividing the above values by the event plane resolution of the corresponding centrality class. The same procedure has been applied in the event-by-event approach of Holopainen et al. [30].

In Fig. 3 we show $v_2(\epsilon_2)$ and $v_3(\epsilon_3)$ for two different centrality classes ($b < 3.4$ fm and $b = 5 - 9$ fm).

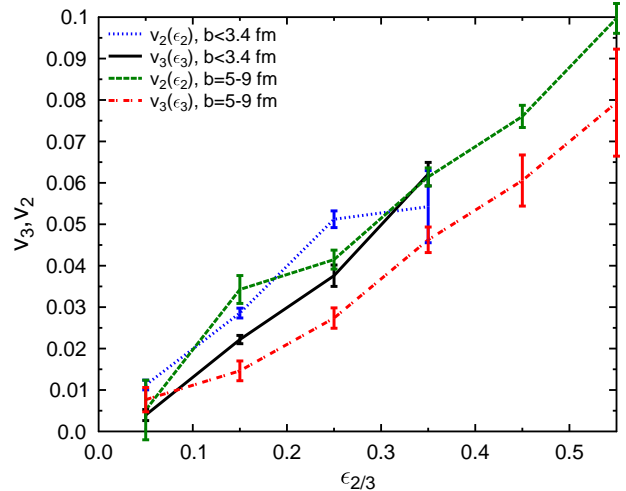


FIG. 3: (Color online) Dependence of v_2 and v_3 on the initial ϵ_2 and ϵ_3 of charged particles in central ($b < 3.4$ fm) and mid-central ($b = 5 - 9$ fm) Au+Au collisions at $\sqrt{s_{NN}} = 200$ A GeV at midrapidity ($|\eta| < 1$).

All the curves behave linearly within error bars, a larger initial eccentricity/triangularity leads to a larger elliptic/triangular flow. For v_3 the translation of the initial anisotropy into the final anisotropy is less efficient for non-central collisions than for central collisions. For elliptic flow the lines have a similar slope, so the elliptic flow response is similar in central and more peripheral collisions.

The impact parameter dependence of the flow coefficients for charged particles is shown in Fig. 4. First of all, the triangular flow has a finite value which exhibits only a weak centrality dependence. This is another hint that v_3 is only induced by fluctuations in contrast to v_2 which has a geometry influence in addition that is centrality dependent. ϵ_2 and ϵ_3 increase as a function of impact parameter since the almond shape of the overlap region gets more pronounced in peripheral collisions and the fluctuations are more important in smaller systems. For the third Fourier coefficient the ratio of v_3/ϵ_3 decreases slightly for more peripheral collisions which reflects the shorter duration of the hydrodynamic evolution. There is less time to translate the initial state anisotropy to a final state momentum anisotropy. Furthermore, the relative elliptic flow is larger than the relative triangular flow, so the transfer of coordinate space anisotropy to momentum space anisotropy is more efficient for lower harmonics than for higher ones. The same result has already been found for v_4 that is much smaller than v_2 [31].

The momentum dependence of v_3 and v_2 for charged particles is shown in Fig. 5. It shows that the elliptic flow is almost twice as large as the triangular flow in mid-central collisions. The elliptic flow results extracted with the event plane method are nonzero even in the most central collisions due to the fluctuations of the participant plane with respect to the reaction plane. In central colli-

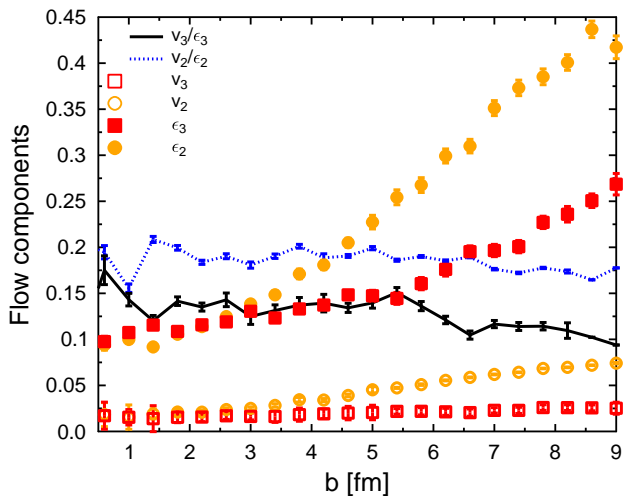


FIG. 4: (Color online) Impact parameter dependence of v_3 (open squares) and v_2 (open circles) of charged particles in Au+Au collisions at $\sqrt{s_{NN}} = 200A$ GeV at midrapidity ($|\eta| < 1$). The full and the dotted line represent the ratios of v_3/ϵ_3 and v_2/ϵ_2 respectively.

sions the magnitude and the shape of the triangular flow is similar to the elliptic flow. This can be traced back to the fact the distribution of spatial event plane angles $P(\Psi_2)$ and $P(\Psi_3)$ are flat in central collisions ($b=0$ fm), rendering no correlation between v_2/v_3 and the reaction plane. The remaining correlation for central collisions (see Fig. 1) of Ψ_2 with the reaction plane arises because there is a contribution from finite impact parameter calculations ($b < 3.4$ fm) in the most central class of events.

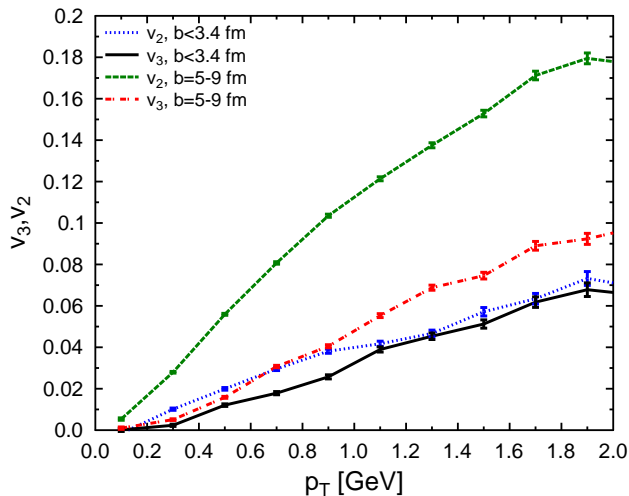


FIG. 5: (Color online) Transverse momentum dependence of v_3 and v_2 of charged particles in central ($b < 3.4$ fm) and mid-central ($b = 5-9$ fm) Au+Au collisions at $\sqrt{s_{NN}} = 200A$ GeV at midrapidity ($|\eta| < 1$).

The transverse momentum dependence of triangular flow for identified particles is shown in Fig. 6. We have checked that the elliptic flow for identified particles is compatible with the experimental data. The fire-

ball created at the highest RHIC energies is dominated by mesons and thus the pion flow is very similar to the charged particle flow. For the protons, the same mass splitting effect is seen for v_3 as for elliptic flow [26]. In addition, the proton v_3 is almost equal for central and mid-central collisions.

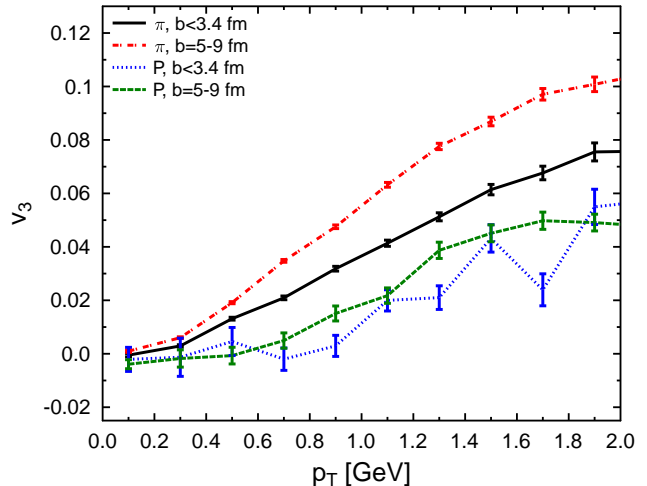


FIG. 6: (Color online) Transverse momentum dependence of v_3 for pions and protons in central ($b < 3.4$ fm) and mid-central ($b = 5-9$ fm) Au+Au collisions at $\sqrt{s_{NN}} = 200A$ GeV at midrapidity ($|\eta| < 1$).

Fig. 7 shows the pseudorapidity dependence of the two flow coefficients for charged particles in two centrality classes. Due to the initial conditions generated by UrQMD with its reliance on fluxtube fragmentation one obtains a long-range $\Delta\eta$ correlation that can be observed in the final state. The elliptic flow results are flat for at least two units of pseudorapidity whereas the triangular flow distribution is almost flat over the whole pseudorapidity range ($\Delta\eta = 4$) covered by the present calculation.

In conclusion, we have presented the first calculation of triangular flow from a (3+1)d ideal hydrodynamics approach in Au+Au collisions at $\sqrt{s_{NN}} = 200A$ GeV. The fluctuating initial conditions and the event-by-event setup are crucial for this observable. By translating initial state triangularity to the final state momentum distributions via pressure gradients a finite value of the third coefficient of the Fourier expansion of the azimuthal distribution of the particles in the final state is generated.

Our method is based on a generalization of the standard event plane analysis that has been used for elliptic flow and can therefore be done in experiments in exactly the same way. While v_2 shows a strong impact parameter dependence, v_3 exhibits only a weak centrality dependence and is close to v_2 in central collisions. The transverse momentum dependence of v_3 is similar to the elliptic flow and also the mass splitting is observed for identified particles. The flat rapidity dependence that results from the color flux tubes in the initial conditions is in agreement with the observation of the ridge in $\Delta\eta$ - $\Delta\phi$ correlations. By measuring v_3 also in a differential way

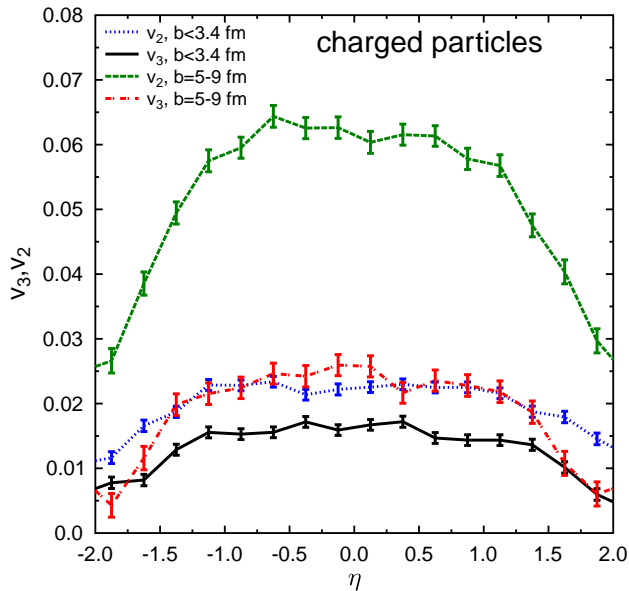


FIG. 7: (Color online) Pseudorapidity dependence of v_3 and v_2 for charged particles in Au+Au collisions at $\sqrt{s_{NN}} = 200A$ GeV.

one might be able to learn something about the amount and the size of the initial state fluctuations.

Acknowledgements

We are grateful to the Open Science Grid for the computing resources. The authors thank Dirk Rischke for providing the 1 fluid hydrodynamics code. H.P. acknowledges a Feodor Lynen fellowship of the Alexander von Humboldt foundation. This work was supported in part by U.S. department of Energy grant DE-FG02-05ER41367 and NSF grant PHY-09-41373. H. Petersen thanks Burak Alver and Michael Mitrovski for fruitful discussions. The authors thank Jean-Yves Ollitrault for his comments to the manuscript. Furthermore, the INT Seattle is acknowledged for support to participate in the program "Quantifying the properties of Hot and Dense QCD matter" where the idea for this publication was born.

-
- [1] J. Y. Ollitrault, Phys. Rev. D **46**, 229 (1992).
[2] S. Voloshin and Y. Zhang, Z. Phys. C **70**, 665 (1996).
[3] P. F. Kolb, J. Sollfrank and U. W. Heinz, Phys. Lett. B **459**, 667 (1999).
[4] D. Teaney, J. Lauret and E. V. Shuryak, Phys. Rev. Lett. **86**, 4783 (2001).
[5] K. H. Ackermann *et al.* [STAR Collaboration], Phys. Rev. Lett. **86**, 402 (2001).
[6] S. S. Adler *et al.* [PHENIX Collaboration], Phys. Rev. Lett. **91**, 182301 (2003).
[7] J. Adams *et al.* [STAR Collaboration], Phys. Rev. Lett. **92**, 052302 (2004).
[8] B. B. Back *et al.* [PHOBOS Collaboration], Phys. Rev. Lett. **94**, 122303 (2005).
[9] J. Adams *et al.* [STAR Collaboration], Nucl. Phys. A **757**, 102 (2005).
[10] P. Romatschke and U. Romatschke, Phys. Rev. Lett. **99**, 172301 (2007).
[11] N. Borghini, P. M. Dinh and J. Y. Ollitrault, Phys. Rev. C **63**, 054906 (2001).
[12] B. Alver and G. Roland, Phys. Rev. C **81**, 054905 (2010).
[13] B. H. Alver, C. Gombeaud, M. Luzum and J. Y. Ollitrault, arXiv:1007.5469 [nucl-th].
[14] J. Takahashi *et al.*, Phys. Rev. Lett. **103**, 242301 (2009).
[15] R. Andrade, F. Grassi, Y. Hama and W. L. Qian, arXiv:0912.0703 [nucl-th].
[16] S. A. Bass *et al.*, Prog. Part. Nucl. Phys. **41**, 255 (1998) [Prog. Part. Nucl. Phys. **41**, 225 (1998)].
[17] M. Bleicher *et al.*, J. Phys. G **25**, 1859 (1999).
[18] H. Petersen, J. Steinheimer, G. Burau, M. Bleicher and H. Stoecker, Phys. Rev. C **78**, 044901 (2008).
[19] H. Petersen and M. Bleicher, Phys. Rev. C **79**, 054904 (2009).
[20] B. Andersson, G. Gustafson, G. Ingelman and T. Sjostrand, Phys. Rept. **97**, 31 (1983).
[21] J. Steinheimer, M. Bleicher, H. Petersen, S. Schramm, H. Stoecker and D. Zschesche, Phys. Rev. C **77**, 034901 (2008).
[22] D. H. Rischke, S. Bernard and J. A. Maruhn, Nucl. Phys. A **595**, 346 (1995).
[23] D. H. Rischke, Y. Pursun and J. A. Maruhn, Nucl. Phys. A **595**, 383 (1995) [Erratum-ibid. A **596**, 717 (1996)].
[24] D. Zschesche, S. Schramm, J. Schaffner-Bielich, H. Stoecker and W. Greiner, Phys. Lett. B **547**, 7 (2002).
[25] J. Steinheimer, V. Dexheimer, H. Petersen, M. Bleicher, S. Schramm and H. Stoecker, Phys. Rev. C **81**, 044913 (2010).
[26] H. Petersen and M. Bleicher, Phys. Rev. C **81**, 044906 (2010).
[27] Q. f. Li, J. Steinheimer, H. Petersen, M. Bleicher and H. Stoecker, Phys. Lett. B **674**, 111 (2009).
[28] A. M. Poskanzer and S. A. Voloshin, Phys. Rev. C **58**, 1671 (1998).
[29] G. Y. Qin, H. Petersen, S. A. Bass and B. Muller, arXiv:1009.1847 [nucl-th].
[30] H. Holopainen, H. Niemi and K. J. Eskola, arXiv:1007.0368 [hep-ph].
[31] and A. Adare [The PHENIX Collaboration], arXiv:1003.5586 [nucl-ex].
[32] The code is available as UrQMD-3.3p1 at <http://urqmd.org>